# Genetic variation in GAD1 is associated with cortical thickness in the parahippocampal gyrus

## Supplementary Materials

## SM 1 Methods and Materials

*SM 1.1 Structural Image Acquisition and Data Processing*

Structural magnetic resonance imaging (sMRI) data was acquired with either a 1.5T Siemens Sonata (UNM, MGH, and UI) or a 3T Siemens Trio (UMN). The T1-weighted structural brain scans at each of the four sites were acquired with a coronal gradient echo sequence: TR=2530 ms for 3T, TR=12 ms for 1.5T; TE=3.79 ms for 3T, TE=4.76 ms for 1.5T; TI=1100 ms for 3T; Bandwidth=181 for 3T, Bandwidth=110 for 1.5T; 0.625×0.625x1.5 $mm^3$ voxel size; slice thickness 1.5 mm; FOV, 256×256×128 cm matrix; FOV=16 cm; NEX=1 for the 3T, NEX=3 for the 1.5T.

Cross-site calibration and reliability of these acquisition sequences for each scanner was established prior to the study (Jovicich et al., 2006; Jovicich et al., 2009; Yendiki et al., 2010).

Processing of the sMRI data included volumetric segmentation and cortical surface reconstruction using FreeSurfer (version 4.0.1) as described previously (Dale, Fischl, & Sereno, 1999; Fischl & Dale, 2000; Fischl et al., 2002). Within the validated and complex FreeSurfer surface reconstruction algorithm, white matter segmentations were produced, topological defects in the surface were automatically corrected and the white and gray matter boundary was tessellated. After intensity normalization, the gray/white matter and the gray/cerebrospinal fluid borders were detected at the location where the greatest shift in intensity defines the transition to the other tissue class (Dale et al., 1999; Fischl, Sereno, & Dale, 1999). Final surfaces were used to calculate cortical thickness at each vertex on the tessellated surface as the closest distance from the gray/white boundary to the gray/cerebrospinal fluid boundary (Fischl et al., 2000). Segmentation and surface reconstruction quality were assured by manual inspection of all raw MRI volumes, segmented volumes in three planes and pial as well as inflated volumes. For additional information on technical details of the manual interventions please refer to the FreeSurfer homepage(http://surfer.nmr.mgh.harvard.edu). One participants' MRI data failed the aforementioned quality assurance due to a segmentation error in the occipital lobe. The data of this subject were subsequently recovered with minor manual intervention according to the FreeSurfer user guidelines.

Entire cortex vertex wise analyses of cortical thickness were performed contrasting A allele carriers vs. G allele homozygotes. Briefly, spherical registered cortical thickness data from all subjects were mapped to an average subject (http://surfer.nmr.mgh.harvard.edu/fswiki/FsAverage). Cortical thickness maps were smoothed using a 10mm full-width-at-half-maximum Gaussian kernel. Finally, general linear models were run at all vertices (n=163 842) per hemisphere. For more intuitive interpretation of our main finding we estimated the actual cortical thickness in millimeter (mm). In order to do so we labeled this cluster region as a region-of-interest (ROI), mapped it back on to each individual subject's unfolded surface by applying the same algorithm that morphed each subject' s unfolded surface to the average spherical surface representation and extracted the average thickness for each individual.

*SM 1.2 Sternberg Item Recognition Paradigm*

The Sternberg Item Recognition Paradigm (SIRP) permits the assessment of the maintenance and scanning components of working memory (Manoach et al., 1999). During SIRP performance, neural activation increases as a function of working memory load (Manoach et al., 2000). In this study, the identical block-design SIRP was used across all 4 acquisition sites as described previously (Roffman et al., 2008). Participants practiced the paradigm before scanning until they understood the task well enough to perform at a greater-than-chance level of accuracy. Briefly, each block began with a 2-second prompt to begin ("learn"), followed by a 6-second presentation of a memory set, composed of one (1t), three (3t), or five (5t) digits, constituting three levels of working memory load (Encode phase). This Encode phase was followed by a 38 -second presentation of 14 digits, one at a time for 1.1 seconds each (the Probe phase). During the Probe phase, participants responded to each probe using a button box to indicate whether or not the probe digit was in the memory set. The participants responded using the thumbs of each hand, with the designated target thumb randomly assigned to the right or left hand. Each of the three runs included two 46-second blocks of each of the three load conditions (Encode-Probe sequence, 6 blocks total/run), presented in a pseudorandom order with the blocks of each condition alternating with fixation epochs (4-20 seconds). Insufficient task performance was defined as a block completed with less than a 75% accuracy rate. One subject met these criteria for four or more of the 18 SIRP blocks and was excluded from the analyses. For more details see previous studies (Ehrlich et al., 2010; Roffman et al., 2008).

*SM 1.3 Functional Image Acquisition and Data Processing*

Functional MRI (fMRI) data was acquired with either a 1.5T Siemens Sonata (UNM) or a 3T Siemens Trio (UI, MGH, and UMN). For all sites, functional images were acquired by using single-shot echo-planar imaging with identical parameters [orientation: AC–PC line; number of slices = 27; slice thickness=4 mm, 1-mm gap; TR=2,000 ms; TE=30ms (3T) or 40ms (1.5T), FOV=22cm; matrix 64×64; flip angle=90°; voxel dimensions = 3.44×3.44×4 $mm^3$]. Functional images were processed using the Functional Bioinformatics Research Network (FBIRN) Image Processing Stream, a pipeline utilizing the FMRIB Software Library of FSL (for details see (Smith et al., 2004)). A Functional Imaging Linear Model (FILM, including temporal whitening(Woolrich, Ripley, Brady, & Smith, 2001) was fit to each subject's preprocessed functional time series for each SIRP run to estimate regression parameters. The haemodynamic response function was modeled as a single gamma function. The magnitude of each contrast of parameter estimates (COPE), along with an estimate of its variability derived from model residuals, was passed to a second-level fixed effects analysis to combine COPE's from separate runs, yielding a composite T-statistic map for each contrast of interest for each subject.

We evaluated the quality of the fMRI data by manual inspection and using artifact detection tools (Whitfield-Gabrieli, 2009). Outlier time frames in each fMRI data time series (detected using the artifact detection tools) were defined by: (1) global mean image intensity that differed by more than 3 standard deviations from the mean of the entire series of time frames in a scan, (2) displacement due to motion by more than 1 mm in the x, y or z direction relative to the previous time frame or (3) rotation due to motion by more than 0.1 rad around any of the three axes relative to the previous time frame. We removed the outlier time frames through the use of nuisance regressors in the linear model. In the case of runs where more than 15% of the time frames were flagged as outliers, the entire run was dropped from the analysis one participant. Manual inspections were used to check for whole-brain coverage of brain masks, motion and global mean intensity outlier timepoints, alignment of structural and functional scans, and registration problems (Epi to T1 and T1 to template).

*SM 1.4 Statistical analyses of the fMRI part*

In our fMRI analyses, we used a COPE that modeled all working memory loads (Probe-1t, Probe-3t and Probe-5t) versus fixation to identify areas with task-induced deactivation. In our final higher level model we tested the effects of genotype in brain regions with robust task-induced deactivation by using a prethreshold mask derived from the main effects model (Z=3). All higher level models were controlled for the effects of acquisition site. Group differences were visualized as z-maps or p-maps, i.e. brainmaps where different colors represent the results of the statistical models as z-values or p-values.

# SM 2 Results

*SM 2.1 Demographics*

The observed genotype frequency of catechol-O-methyltransferase (COMT)Val158Met did not deviate from Hardy Weinberg equilibrium ($\chi^2$=0.38, df=1, p=0.54). Demographic variables such as age, sex, ethnicity, parental socioeconomic status, wide range achievement test and handedness according to the Annett Handedness scale did not differ across the Val158Met genotype groups (Table S1) and Chi-square statistics did not reveal any relationships between genotype group and acquisition site ($\chi^2$=11.01, df=6, p=0.088).

*SM 2.2 fMRI results*

On a more exploratory level, we tested for associations between glutamic acid decarboxylase 1 (GAD1) and neuronal activity. Our findings from the cortical thickness analyses suggest GAD1-associated differences in important nodes of the default mode network (DMN) (listed below) (Buckner, Andrews-Hanna, & Schacter, 2008; Raichle et al., 2001). Thus, in our exploratory fMRI analyses in the same cohort of healthy controls we focused on task-induced deactivation areas during the SIRP working memory task. Besides robust activations in typical working memory-related brain areas (see Figure S2) we saw task-induced deactivation in brain regions associated with the DMN, i.e. the ventral medial prefrontal cortex, dorsal medial prefrontal cortex, posterior cingulate, inferior parietal lobule, the lateral temporal cortex and the hippocampal formation including the parahippocampal gyrus (PHG) ((Buckner et al., 2008), see Figure S3). When contrasting GAD1 rs3749034 G allele homozygotes with A Carriers we found a reduced task-induced deactivation in Brodmann area 25 bilaterally in G allele homozygotes (Figure S4). There was no association between rs3749034 genotype and SIRP performance, i.e. % accuracy during working memory task performance (t=-0.145, df=91, p=0.885). No significant interactions between the GAD1 rs3749034 SNP and the COMT Val158Met Polymorphism were observed in our fMRI analyses.

# SM 3 Discussion

*SM 3.1 - GAD1 and reduced task-induced deactivation during working memory*

The GABAergic system has been previously linked to the DMN. Combining fMRI and magnetic resonance spectroscopy it has been shown that higher concentrations of GABA in the

anterior cingulate gyrus, one of the key regions of the DMN, were specifically correlated with more pronounced task-induced deactivation in the very same region (Northoff et al., 2007). This may indicate that GABA specifically modulates task-induced deactivation which can be interpreted as neuronal inhibition (Devor et al., 2007). Our own finding of reduced deactivation during working memory performance in G/G risk -homozygotes is located in Brodmann area 25, i.e. the subgenual area and parts of the subgenual cingulate cortex. These regions belong to the medial prefrontal cortex which is a major hub of the DMN (Buckner et al., 2009). We therefore suggest that GAD1 as a key component of GABAergic functioning may contribute to the disturbed DMN activation observed in schizophrenia.

## References:


Buckner, R. L., Andrews-Hanna, J. R., & Schacter, D. L. (2008). The brain's default network: anatomy, function, and relevance to disease. *Ann N Y Acad Sci* **1124,** 1-38.

Buckner, R. L., Sepulcre, J., Talukdar, T., Krienen, F. M., Liu, H., Hedden, T., Andrews-Hanna, J. R., Sperling, R. A., & Johnson, K. A. (2009). Cortical hubs revealed by intrinsic functional connectivity: mapping, assessment of stability, and relation to Alzheimer's disease. *J Neurosci* **29,** 1860-73.

Dale, A. M., Fischl, B., & Sereno, M. I. (1999). Cortical surface-based analysis. I. Segmentation and surface reconstruction. *Neuroimage* **9,** 179-94.

Devor, A., Tian, P., Nishimura, N., Teng, I. C., Hillman, E. M., Narayanan, S. N., Ulbert, I., Boas, D. A., Kleinfeld, D., & Dale, A. M. (2007). Suppressed neuronal activity and concurrent arteriolar vasoconstriction may explain negative blood oxygenation level-dependent signal. *J Neurosci* **27,** 4452-9.

Ehrlich, S., Morrow, E. M., Roffman, J. L., Wallace, S. R., Naylor, M., Bockholt, H. J., Lundquist, A., Yendiki, A., Ho, B. C., White, T., Manoach, D. S., Clark, V. P., Calhoun, V. D., Gollub, R. L., & Holt, D. J. (2010). The COMT Val108/158Met polymorphism and medial temporal lobe volumetry in patients with schizophrenia and healthy adults. *Neuroimage* **53,** 992-1000.

Fischl, B., & Dale, A. M. (2000). Measuring the thickness of the human cerebral cortex from magnetic resonance images. *Proc Natl Acad Sci U S A* **97,** 11050-5.

Fischl, B., Salat, D. H., Busa, E., Albert, M., Dieterich, M., Haselgrove, C., van der Kouwe, A., Killiany, R., Kennedy, D., Klaveness, S., Montillo, A., Makris, N., Rosen, B., & Dale, A. M. (2002). Whole brain segmentation: automated labeling of neuroanatomical structures in the human brain. *Neuron* **33,** 341-55.

Fischl, B., Sereno, M. I., & Dale, A. M. (1999). Cortical surface-based analysis. II: Inflation, flattening, and a surface-based coordinate system. *Neuroimage* **9,** 195-207.

http://surfer.nmr.mgh.harvard.edu.

Jovicich, J., Czanner, S., Greve, D., Haley, E., van der Kouwe, A., Gollub, R., Kennedy, D., Schmitt, F., Brown, G., Macfall, J., Fischl, B., & Dale, A. (2006). Reliability in multi-site structural MRI studies: effects of gradient non-linearity correction on phantom and human data. *Neuroimage* **30,** 436-43.

Jovicich, J., Czanner, S., Han, X., Salat, D., van der Kouwe, A., Quinn, B., Pacheco, J., Albert, M., Killiany, R., Blacker, D., Maguire, P., Rosas, D., Makris, N., Gollub, R., Dale, A., Dickerson, B. C., & Fischl, B. (2009). MRI-derived measurements of human subcortical, ventricular and intracranial brain volumes: Reliability effects of scan sessions, acquisition sequences, data analyses, scanner upgrade, scanner vendors and field strengths. *Neuroimage* **46,** 177-92.

Manoach, D. S., Gollub, R. L., Benson, E. S., Searl, M. M., Goff, D. C., Halpern, E., Saper, C. B., & Rauch, S. L. (2000). Schizophrenic subjects show aberrant fMRI activation of dorsolateral prefrontal cortex and basal ganglia during working memory performance. *Biol Psychiatry* **48,** 99-109.

Manoach, D. S., Press, D. Z., Thangaraj, V., Searl, M. M., Goff, D. C., Halpern, E., Saper, C. B., & Warach, S. (1999). Schizophrenic subjects activate dorsolateral prefrontal cortex during a working memory task, as measured by fMRI. *Biol Psychiatry* **45,** 1128-37.

Northoff, G., Walter, M., Schulte, R. F., Beck, J., Dydak, U., Henning, A., Boeker, H., Grimm, S., & Boesiger, P. (2007). GABA concentrations in the human anterior cingulate cortex predict negative BOLD responses in fMRI. *Nat Neurosci* **10,** 1515-7.

Raichle, M. E., MacLeod, A. M., Snyder, A. Z., Powers, W. J., Gusnard, D. A., & Shulman, G. L. (2001). A default mode of brain function. *Proc Natl Acad Sci U S A* **98,** 676-82.

Roffman, J. L., Gollub, R. L., Calhoun, V. D., Wassink, T. H., Weiss, A. P., Ho, B. C., White, T., Clark, V. P., Fries, J., Andreasen, N. C., Goff, D. C., & Manoach, D. S. (2008). MTHFR 677C --> T genotype disrupts prefrontal function in schizophrenia through an interaction with COMT 158Val --> Met. *Proc Natl Acad Sci U S A* **105,** 17573-8.

Smith, S. M., Jenkinson, M., Woolrich, M. W., Beckmann, C. F., Behrens, T. E., Johansen-Berg, H., Bannister, P. R., De Luca, M., Drobnjak, I., Flitney, D. E., Niazy, R. K., Saunders, J., Vickers, J., Zhang, Y., De Stefano, N., Brady, J. M., & Matthews, P. M. (2004). Advances in functional and structural MR image analysis and implementation as FSL. *Neuroimage* **23 Suppl 1,** S208-19.

Whitfield-Gabrieli, S. (2009). Artifact Detection Tools. http://web.mit.edu/swg/software.htm.

Woolrich, M. W., Ripley, B. D., Brady, M., & Smith, S. M. (2001). Temporal autocorrelation in univariate linear modeling of FMRI data. *Neuroimage* **14,** 1370-86.

Yendiki, A., Greve, D. N., Wallace, S., Vangel, M., Bockholt, J., Mueller, B. A., Magnotta, V., Andreasen, N., Manoach, D. S., & Gollub, R. L. (2010). Multi-site characterization of an fMRI working memory paradigm: reliability of activation indices. *Neuroimage* **53,** 119-31.

## Table:

| Val158Met (rs4680) | | | Val/Val carriers (n=25) | Val/Met carriers (n=44) | Met/Met carriers (n=25) | $\chi^2$/F | df/ $df_M$, $df_R$ | p |
|---|---|---|---|---|---|---|---|---|
| Sex | female | N | 9 | 24 | 7 | 5.194 | 2 | 0.075 |
| | | % | 36 | 54.5 | 28 | | | |
| Ethnicity | white | N | 23 | 37 | 24 | 1.25 | 2 | 0.534 |
| | | % | 92 | 84.1 | 96 | | | |
| Age | | Mean (SD) | 34.36 (11.45) | 32.32(10.95) | 34.64(11.83) | 0.438 | 2, 91 | 0.646 |
| WRAT | | Mean (SD) | 51.36(4.97) | 50.73(4.15) | 49.88(2.41) | 0.78 | 2, 91 | 0.462 |
| Parental SES | | Mean (SD) | 2.72(0.74) | 2.77(0.74) | 2.6(0.71) | 0.445 | 2, 91 | 0.642 |
| Handedness | | Mean (SD) | 0.64(2.41) | 1.61(3.64) | 0.56(1.23) | 1.471 | 2, 91 | 0.235 |

Table S1. Basic demographics are presented according to COMT Val158Met genotype. WRAT, Wide Range Achievement Test; SES, socioeconomic status; Handedness, Annett Handedness Scale. One way ANOVA did not show any significant main effects of genotype group on Age, WRAT Score, Parental SES and Handedness. Chi-square statistics did not reveal any relationships between genotype groups and Gender and Ethnicity.

## Figures:

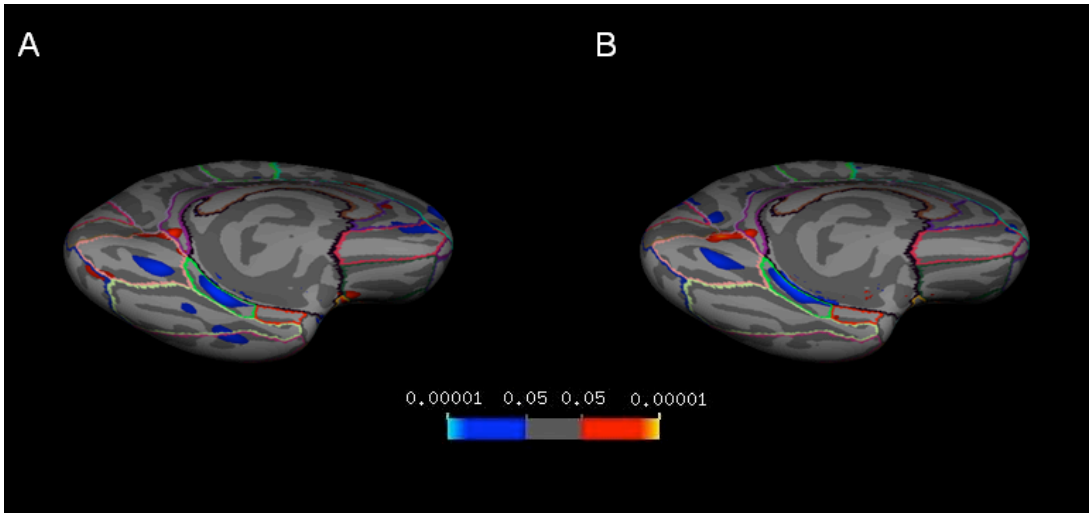


Figure S1. Cortical statistical maps illustrating the region of reduced cortical thickness in G allele homozygotes compared to A carriers A) in the Caucasian subgroup and B) in the right-handed subgroup at a threshold of p<0.05 (uncorrected).

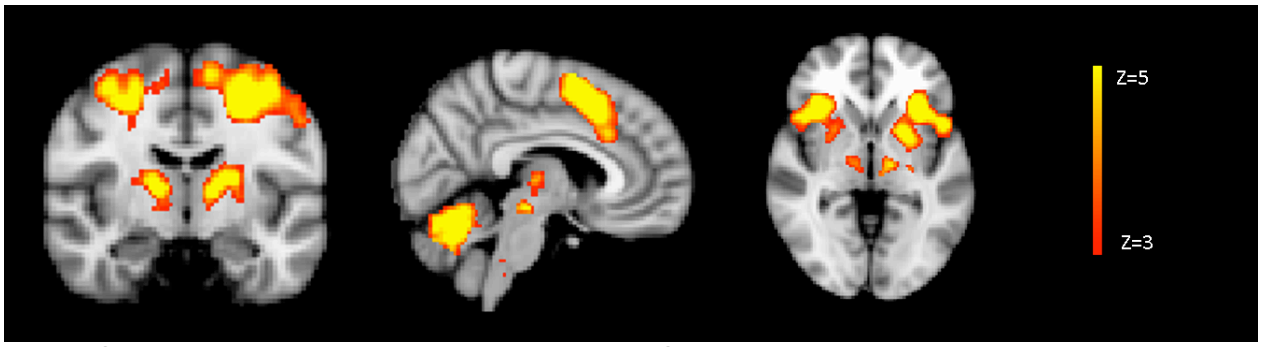


Figure S2. Task-induced neural activity during the SIRP (p=0.001, uncorrected). In line with previous studies, participants showed robust bilateral activations in the DLPFC, intraparietal sulcus, premotor, motor and sensory cortex during the SIRP working memory task (Manoach et al., 2000).

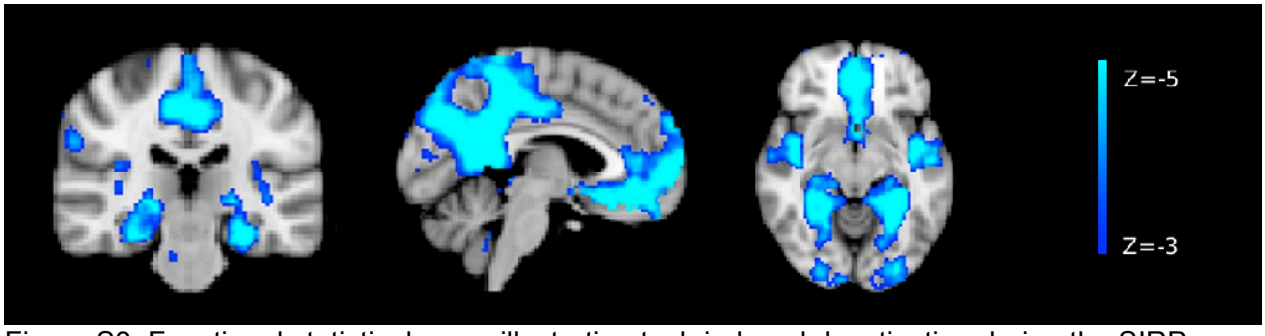


Figure S3. Functional statistical maps illustrating task-induced deactivation during the SIRP (p<0.001, uncorrected for 10 contiguous voxels).

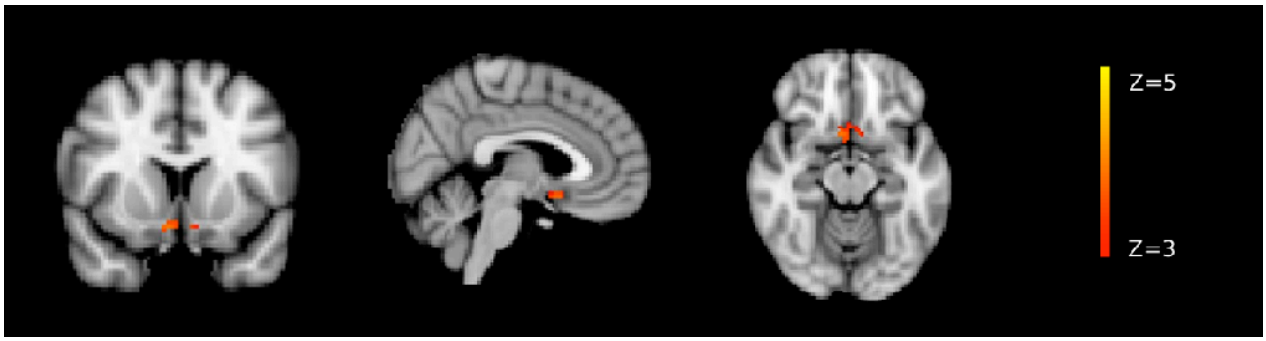

Figure S4. Functional statistical maps demonstrating reduced task-induced deactivation in GAD1 rs3749034 G allele homozygotes compared to A carriers during SIRP ($p<0.001$, uncorrected for 10 contiguous voxels, z-max=3.89 at x=6, y=12 and z=-14).